Available online at www.sciencedirect.com
SCIENCE DIRECT®
C. R. Physique 4 (2003) 231–239
COMPTES RENDUS PHYSIQUE

Hydrodynamics and physics of soft objects/Hydrodynamique et physique des objets mous

Mechanical instability induced by complex liquid desiccation

Instabilité mécanique induite par séchage de liquides complexes

Ludovic Pauchard *, Catherine Allain

Laboratoire FAST (Unité Mixte de Recherche Paris VI, Paris XI, et CNRS: UMR 7608), bâtiment 502, campus Universitaire, 91405 Orsay cedex, France

Presented by Guy Laval

Abstract

The drying of sessile drops of a complex liquid can lead to various types of surface distortion and final shapes. Here we investigate the desiccation of drops for two different systems: colloidal particle suspensions and polymer solutions. During solvent loss, the non-volatile compounds accumulate near the vapor/drop interface and, depending on the experimental conditions, they can form a permeable rigid skin (a gelled or glassy skin) displaying a buckling instability. In some cases secondary instabilities also take place. Although the nature and the physicochemical properties of the two systems are quite different, the shape evolutions show a remarkable similarity. A good agreement is found with a description based on the comparison of the characteristics times involved in the problem. ***To cite this article: L. Pauchard, C. Allain, C. R. Physique 4 (2003).***

Résumé

Au cours du séchage, des gouttes de liquides complexes, déposées sur un substrat, peuvent subir des déformations variées conduisant à différentes morphologies finales. Nous nous intéressons ici au séchage de gouttes de deux systèmes différents : une suspension de particules colloïdales et une solution de polymères. Au cours de l'évaporation du solvant, les composés non volatiles s'accumulent près de l'interface vapeur/goutte et, en fonction des conditions expérimentales, il peut se former une « croûte » rigide (gélifiée ou vitreuse) qui subit une instabilité de flambement. Dans certains cas, des instabilités secondaires apparaissent. Bien que la nature et les propriétés physico-chimiques des deux systèmes soient différentes, les évolutions des morphologies rencontrées présentent une similarité remarquable. Une description, basée sur la comparaison des temps caractéristiques intervenant dans le processus, est en bon accord avec les résultats obtenus. ***Pour citer cet article : L. Pauchard, C. Allain, C. R. Physique 4 (2003).***

1. Introduction

The evaporation of a sessile drop is not only important in heat transfer applications but is also involved in many common and everyday phenomena, such as for instance, the ring-like spots remaining on dishes that have been left drying, or the enhanced

* Corresponding author.
E-mail address: pauchard@ariane.fast.u-psud.fr (L. Pauchard).

1631-0705/03/$ – see front matter
doi:10.1016/S1631-0705(03)00027-6

edges in water colour paintings. Recently, there has been a renewed interest for this phenomenon and new important applications have emerged.

Following the amount of non-volatile solutes (salts, macromolecules, colloidal particles, etc.) in the drop liquid, different types of evolution are observed. If this amount is very small, the drop is expected to evaporate with a constant contact angle whose value is determined by surface tension equilibrium. However this occurs only in the ideal case of ultra pure solvents and well cleaned surfaces. In general, the drop's three-phase line is pinned due to a rapid deposition and adhesion of the non-volatile species on the substrate at the drop edge; the drop then evaporates with a constant surface of contact with the substrate. This self-pinning is responsible of an outward flow toward the contact line, which is required for solvent mass conservation. This outward flow convects the non-volatile solutes toward the contact line where they accumulate and deposit leading to the formation of a ring [1–7]. Depending on the nature and concentration of the non-volatile species and on the properties of the substrate, the contact line can move, remaining pinned at a same position during a more or less long time; successive rings are then formed. In most case, the three phase line however remains pinned at its initial location during all the drying; then the outward flow can transfer almost all the non-volatile species to the contact line. This segregation, which is undesirable in some applications, can also be a useful tool, for instance in nanotechnology including variants of lithography (fabrication of nano-dot or nano-ring arrays) [8], production of nano-wires [9], or for various biological applications (formation of DNA or protein deposits, DNA stretching, ...) [10,11].

When the amount of the non-volatile solutes is large (typically for volume fraction larger than 10^{-1}), the drop three phase line also remains pinned at its initial position but the final deposit is too voluminous to only form a ring and a continuous film with a more or less complicated shape forms [2,12–16]. This situation, which is more frequently encountered in practical applications, is complicated due to the numerous coupled phenomena that are involved. During the evaporation the drop shape is mainly governed by two effects: the evolution of the rheological properties on one hand and the occurrence of instabilities on the other. Indeed, when the solutes concentrations increase, the medium follows a 'drying line' across the composition diagram and can undergo for instance a sol-gel transition or a glass transition. In both cases the rheological properties change: the initially fluid medium transforms in a viscoelastic or brittle solid. Moreover, during the evaporation, the solute concentrations are not uniform inside the drop. So the rheological properties vary from one point to another. Coupled with the contact line pinning, this results in a complex drop shape evolution. In a previous work we have investigated the case of charged colloidal suspensions [2,12,17]. The outward flow is responsible of the formation a gelled 'foot' near the contact line while the centre of the drop remains fluid. With time the central cap radius decreases as the foot advances. A similar shape evolution has been

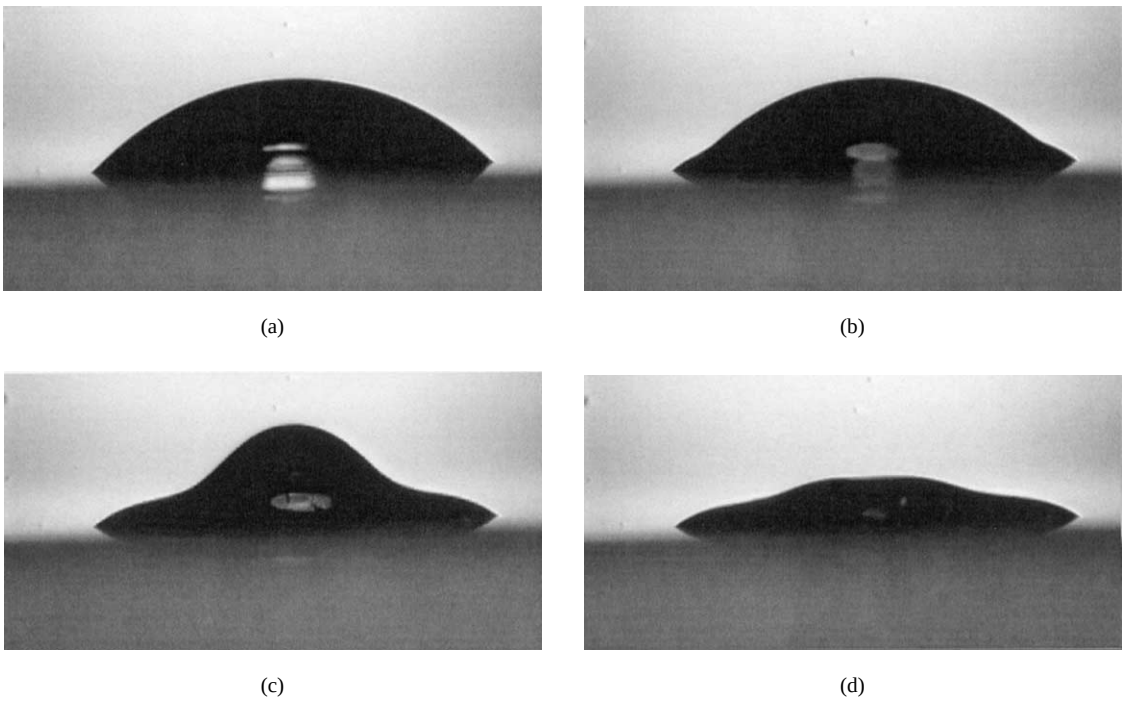

Fig. 1. Digitalized images in lateral views showing the evolution of a drop of silica particle suspension deposited on a glass slide (the drop base diameter is 4 mm); (a) just after the deposition, the drop has a spherical cap shape; (b) a gelled foot forms near the three-phase line while the central part progressively flattens; (c) the apex height has increased and reaches a maximum value; (d) at final stage, the drop has collapsed.

observed in different colloidal systems [16,18]. If the suspension ionic strength in the charged colloidal suspension is increased, the gelation time is decreased and it can be of the order of or even smaller than the drying characteristic time; very different shape evolutions are then found [13]. During the drop drying, different types of instability can also take place due to temperature gradient (the solvent evaporation cools the drop surface) or/and solute concentration gradients; the resulting Rayleigh Bénard or Bénard Marangoni instabilities then modify the shape evolution [14,19–21]. Finally, the stresses resulting of the solvent evaporation can lead to cracking of the drop parts that had transformed in a brittle solid [13,16–18,22,23].

In the present paper, we report on a new type of instability which occurs when the physicochemical conditions are such as a rigid 'skin' forms at the drop surface. Indeed, as this 'skin' behaves like an elastic shell which does not however impede the evaporation, a buckling instability may take place: the shell bends under the decrease of the volume that it encloses while its surface remains constant. A typical example of an unstable evolution is given in Fig. 1. Just after deposition (Fig. 1(a)), the drop has a spherical cap shape; during a first stage (Fig. 1(b)), the evaporation leads to the formation of a gelled foot near the contact line while the central part, which is fluid, progressively flattens. Instead of a continuous evolution, at a given time the apex height stops decreasing, increases and reaches a maximum value that can be larger than its initial value (Fig. 1(c)). At the end of the evaporation (Fig. 1(d)) the drop is collapsed.

We have investigated the occurrence of this shape instability in two different systems: silica colloidal suspensions and solutions of a polymer (dextran) which is glassy at room temperature. In spite of their differences in nature and physicochemical properties, we observe the same type of shape instability for the two systems. The characteristic time when the drop surface begins to distort has been measured as a function of the physicochemical conditions (ionic strength, polymer concentration, ...) and it has been compared with the other characteristic times involved: the drying time, the gelation time and the time of glassy skin formation. In some cases secondary instabilities take place which break or not the axisymetry of the drop.

2. Experimental

The first system is suspensions made of thin silica particles (15 ± 2 nm in diameter) in water. The particle volume fraction was kept constant, $\Phi_p = 0.20$, and the ionic strength, I_s, was adjusted between 0.04 mol/L and 0.6 mol/L. The pH of the suspensions is basic (about 9). So the particles surface bears a high negative charge and DLVO (Derjaguin–Landau–Vervey–Overbeck) theory applies: the colloidal interaction between the particles strongly depends on the ionic strength. For the lower value of I_s the suspension is stable for several months while at large value of I_s the particles aggregate and a colloidal gel forms. Rheological measurements were performed to determine the gelation time, t_G, i.e., the time elapsed between the sample preparation and the gelation transition which corresponds to the divergence of the viscosity and the appearance of an elastic behaviour (see Fig. 2(a)). The gelation time strongly depends on the ionic strength: the larger the ionic strength is, the shorter t_G is. Typically we find $t_G = 5 \times 10^3$ s for $I_s = 0.20$ mol/L and $t_G = 10^3$ s for $I_s = 0.40$ mol/L. Practically, the samples are prepared from a same stock suspension ($\Phi_p = 0.24$, $I_s = 0.04$ mol/L) by adding the volume of a NaCl solution necessary to

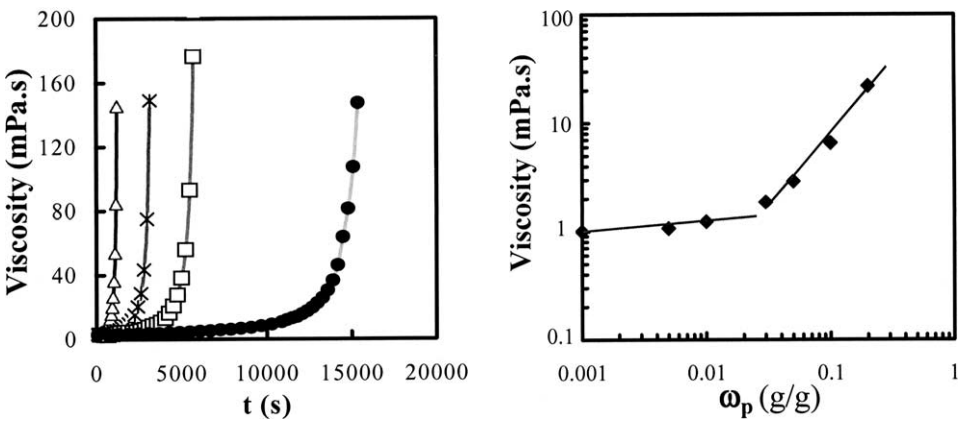

(a) (b)

Fig. 2. Rheological characterizations: (a) Viscosity versus time of colloidal suspensions for different ionic strengths; $I_s = 0.30$ mol/L (△); $I_s = 0.24$ mol/L (×); $I_s = 0.20$ mol/L (□); $I_s = 0.17$ mol/L (●). Note that for the low shear rates used (lower than 10^{-1} s^{-1}) the results do not depend on the imposed shear rate. (b) Viscosity of dextran solutions versus concentration. The grey lines only guide eyes. Measurements were done with an imposed shear rate rheometer (Contraves LS30).

obtain a suspension of volume fraction $\Phi_p = 0.20$ and having the wanted ionic strength I_s. In desiccation experiments, the drop is deposited on the substrate as soon the suspension have been prepared; so drying and gelation begin simultaneously.

The second system is concentrated solutions of dextran, a non-ionic hydrosoluble polysaccharide (Sigma Aldrich Chemical Company). The average molecular weight is 77 000 g/mol (about 200 monomers). The solutions were prepared by dissolving the polymer in pure water (Milli-Ro). Viscosity measurements were performed as a function of the polymer concentration, ω_p (Fig. 2(b)). At low ω_p values, the viscosity increases very slowly and the intrinsic viscosity, evaluated to $[\eta] \cong 27$ g/g, is in agreement with that expected [24]. Above the overlap threshold, $\omega_p^* \cong 0.03$ g/g, as usual in polymer solutions the viscosity increases significantly. The polymer concentration of the solutions used in the desiccation experiments is always larger than ω_p^* so the polymer chains are entangled (semi-dilute regime). On another hand, pure dextran polymer (in the absence of solvent) exhibits a glass transition at a temperature of the order of 220 °C (determined by DSC). The glass transition temperature of a polymer solution is lower than the pure polymer one and decreases as polymer concentration ω_p decreases [25]. Thus, at a given temperature, T_{exp}, the solution has a glass transition temperature smaller than T_{exp} when the polymer concentration is small and a glass transition temperature larger than T_{exp} when the polymer concentration is large. So, it exists a concentration ω_{pg} such kind of solutions are fluid when $\omega_p < \omega_{pg}$ and glassy when $\omega_p > \omega_{pg}$. During solvent evaporation, as the polymer concentration increases, the solution initially fluid becomes glassy.

The geometry used for desiccation consists in drops deposited on a horizontal plate. The substrate is a glass microscope slide (Menzel–Gläser) carefully cleaned with pure water then ethanol before being dried in a heat chamber at 100 °C. The preparation, in particular the time spent at high temperature, has a large influence on the contact angle; that enables to vary it. The substrate is cooled down at room temperature at least 15 minutes before to be put on a support having fine movements by controlled displacements in the three directions of space; this device enables a precise settling and a good centering of the drop with regards to the two cameras that allows accurate observations both in side and top views. The analysis of the first profile recorded after drop deposition enables to determine the initial geometrical characteristics of the drop (R_0 the radius of the contact base, θ_0 the contact angle and H_0 the apex height). After having verified the drop axisymetry from the top view, the drop volume, V, and the surface area, S, at different times are calculated from the drop profile. Spatio-temporal diagrams are also constructed to obtain the apex height variations as a function of time. The set-up is placed inside a glove box in which the room temperature is fixed at 20 °C and the relative humidity, RH, is maintained at a constant value varying in the range from 20% to 80%.

To characterize the drying kinetics we introduce the time, t_D, which describes the rate of volume variations: $t_D^{-1} = -1/V_0(\partial V/\partial t)_{t=0}$. Practically, t_D is calculated from the linear variation of V versus t. Time t_D gives an order of magnitude of the time needed to dry the drop and thus it depends on the relative humidity and on the drop size and contact angle.

3. Results

3.1. Drop shape characterization

The unstable evolution shown in Fig. 1 can be characterized by the superposition of the profiles recorded at different times during desiccation. Figs. 3(a) and 3(b) display respectively the evolution of a drop of silica suspension and that of a drop of dextran solution under the same conditions of temperature, relative humidity and initial contact angle (T of the order of 20 °C; RH of the order of 50%; θ_0 of the order of 30 °). Although the systems are quite different the drop shape evolutions are remarkably similar except at large time ($t > 900$ s). In the case of a silica suspension drop the apex height increases until reaching a maximum value and then a collapse of the drop rapidly takes place. For a dextran solution drop the same evolution is observed but no collapse occurs at large time.

To characterize the beginning of the instability we have investigated the variations of the apex height: $(H - H_0)/H_0$ as a function of dimensionless time t/t_D is reported in Fig. 4 for several drops of colloidal particles suspensions of ionic strength in the range [0.04–0.60 mol/L] and polymer solutions of concentrations in the range [0.20–0.40 g/g]. In the cases of the particles suspension at small ionic strength ($I_s = 0.04$ mol/L) and of the polymer solution at low concentration ($\omega_p = 0.20$ g/g) a regular decrease of the apex height occurs until final stage. This decrease is identical for both systems and is analogous to the case of a pure water drop whose three phase line is pinned. The lateral views of these drops do not display any distortions. For larger ionic strengths or polymer concentrations, the first stages of $(H - H_0)/H_0$ variations are equivalent: after a continuous decrease, $(H - H_0)/H_0$ stops decreasing at a certain time (defined as t_B in the following) and then steeply increases until a maximum value that possibly reaches a value larger than 1: at this time lateral views display strong distortions of the drop profile with the formation of a 'Mexican hat' shape ($t_B = 250$ s in the case of Fig. 3(a) and 700 s in Fig. 3(b)). In a final stage, whereas the apex height of polymer solution drops slowly decreases with time, a rapid collapse occurs for drops of colloidal particles suspensions. The spatio-temporal diagrams (Fig. 4) also show that the relative quantity of water lost by the drop at the buckling time, i.e., t_B/t_D increases when the polymer concentration is lower or the ionic strength is lower.

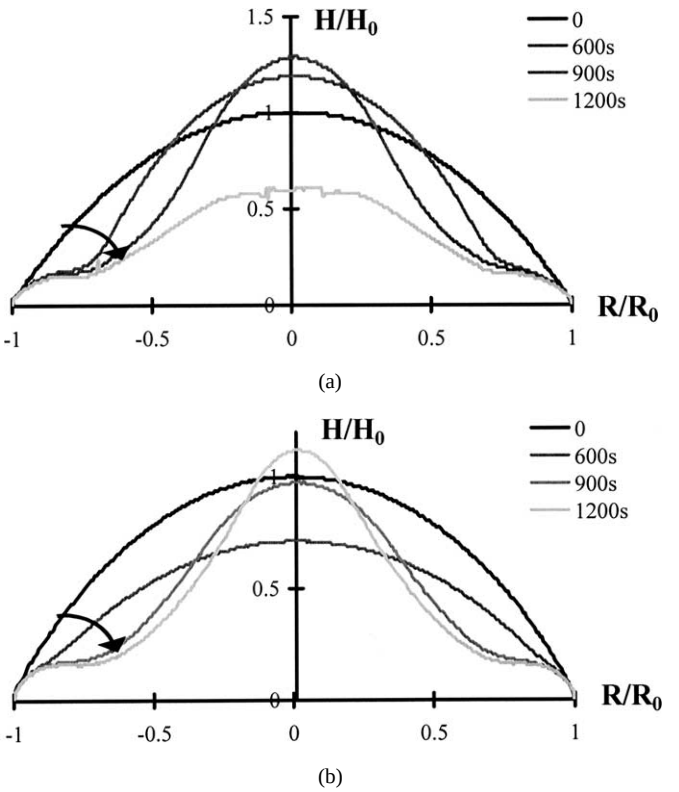

Fig. 3. Dimensionless profiles of drops recorded and superposed at different times: (a) silica particles suspension at $\Phi_p = 0.20$ and $I_s = 0.40$ mol/L; (b) dextran solution at $\omega_p = 0.40$ g/g.

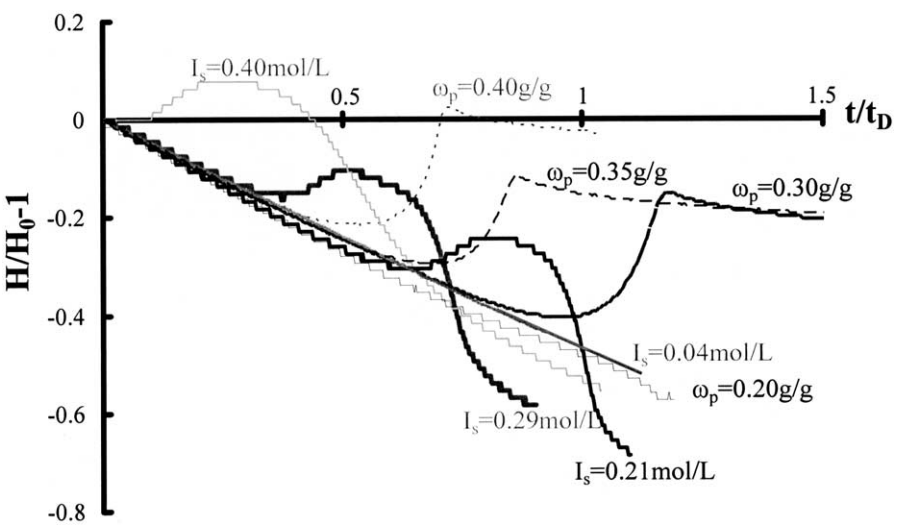

Fig. 4. Dimensionless apex height, $(H - H_0)/H_0$ (H_0 being the drop apex height at $t = 0$) versus dimensionless time, t/t_D. While the less concentrated dextran solution, $\omega_p = 0.20$ g/g (respectively $I_s = 0.04$ mol/L for the colloidal suspension) displays a continuous flattening, the concentrated solutions, $\omega_p = 0.25, 0.30, 0.35$ and 0.40 g/g ($I_s = 0.21, 0.29$ and 0.40 mol/L, respectively, for the colloidal suspension) show a shape instability.

During the first regular decrease of $(H - H_0)/H_0$, the drop shape is not strongly modified and the volume and the surface area calculated from the profile measurements decrease linearly with time. After time t_B, i.e., when the apex height evolution differs from the regular variation the profiles distort and the surface area remains constant while the volume keeps decreasing

but in a slower way. For the two studied systems we have observed that a rigid skin had then formed at the drop surface (we use a simple test that consists in trying to suck up the drop using a micropipette). In the case of colloidal particles suspensions, the skin is formed by a colloidal gel. Under desiccation, the solvent flows through this skin that behaves as a porous medium allowing water transport. So the volume included inside the skin decreases while its area remains constant. In the case of polymer solutions, the rigid skin is a glassy skin. Indeed, due to the increase of the polymer concentration, the drop surface becomes glassy when ω_p reaches ω_{pg}. Once formed, evaporation still continues by solvent diffusion through the glassy polymer skin. So in both cases a rigid skin forms which behaves as an elastic shell but which does not impede evaporation; under solvent loss, the enclosed volume decreases leading to a buckling instability.

In both systems the instability occurrence and its beginning time depend on several physical parameters:

- geometrical parameters: radius of the contact base of the drop, R_0, and contact angle, θ_0, of the drop deposited on the substrate;
- parameters related to the desiccation process: relative humidity, RH, in air surrounding the drop governing the flux of solvent into air;
- physicochemical properties of system: polymer concentration, ω_p, or ionic strength, I_s, for charged colloidal suspensions.

3.2. Instability criterion

To interpret these results and to model the conditions for instability occurrence, we compare the different characteristic times involved. First let us derive the expressions of the drying time, t_D. Under our experimental conditions (absence of convection in the vapour) the transfer of water in air is limited by diffusion. In this way, the evaporation rate writes as [12,17]:

$$W_{E0} = \left(D_w \frac{n_{wsat}}{n_l}\right) A(\theta_0) \frac{(1 - RH)}{R_0}, \tag{1}$$

where D_w is the diffusion coefficient of water into air, n_{wsat} is the water concentration in air at equilibrium with the drop fluid (practically n_{wsat} is almost the same as for pure water), n_1 the number of water mole per unit volume in liquid water and $A(\theta_0)$ a numerical factor related to the shape of the isoconcentration curves of water in air ($A(\theta_0)$ varies only slightly with θ_0, typically from 1.3 to 1 when θ_0 increases from 20 to 90 °). Time t_D is expressed as:

$$t_D = \frac{1}{W_{E0}} \frac{V_0}{S_0}. \tag{2}$$

At constant θ_0 and RH, t_D increases with R_0 following a power law with an exponent 2 in good agreement with previous experiments [12,17,26]. Note also that at constant R_0, Eq. (2) predicts that t_D increases when θ_0 or RH increases. Using tabulated values of the different quantities we can calculate t_D/R_0^2 as a function of polymer concentration and ionic strength. A good agreement is found with our experimental results (see Fig. 5).

Let us now first consider the case of the polymer solutions and derive the expression of t_S, the time corresponding to the formation of a glassy skin, i.e., when the polymer volume fraction at the drop surface, φ_{ps}, becomes equal to the glass transition polymer volume fraction. Setting that at t_S, φ_{ps} equals φ_{pg} and assuming that the evaporation rate is constant and determined by water diffusion in air, we find:

$$t_S = \frac{D_m(\varphi_{pg} - \varphi_p)^2}{W_{E0}^2} \propto \frac{(\varphi_{pg} - \varphi_p)^2}{(1 - RH)^2} R_0^2, \tag{3}$$

where D_m is the polymer/solvent mutual diffusion coefficient. Time t_S will increase when the evaporation rate decreases, i.e., when R_0 or RH increases. In the same way as for t_D, the dependence of t_S on R_0 is given by a power law with an exponent 2 in good agreement with previous results [26]. Using classical values for the involved parameters, the t_S/R_0^2 variation is plotted as a function of the polymer concentration, ω_p, in Fig. 5(a). Moreover experimental measurements, t_B/R_0^2, determined from the spatio-temporal diagrams (Fig. 4) are plotted in Fig. 5(a). Comparing t_S/R_0^2 and t_B/R_0^2 shows a good accordance between the two values; thus in the following we can assume that the buckling instability occurs as soon as the rigid skin forms at the drop surface that is $t_B \equiv t_S$. Comparing the two characteristic times, t_S and t_D, allows the determination of the condition for buckling instability occurrence. Indeed, if $t_D < t_S$, the drop is dried before a glassy skin forms. Under this condition, experiments show that the drop progressively flattens under solvent evaporation, the height of the apex decreasing regularly (case $\omega_p = 0.20$ g/g in Fig. 4). In the final state, a flat 'pancake' is observed with, for the lowest concentrations, a depressed zone in its center. If $t_D > t_S$, buckling instability takes place during drying. Thus the limit of the stability domain is set by $t_S = t_D$. This condition is in agreement with the experimental result (see Fig. 5(a)).

Let us now consider the case of silica particles suspensions. The evaluation of the time when a gelled skin forms is complicated since gelation kinetics strongly depends both on particle volume fraction and on the ionic strength and thus a

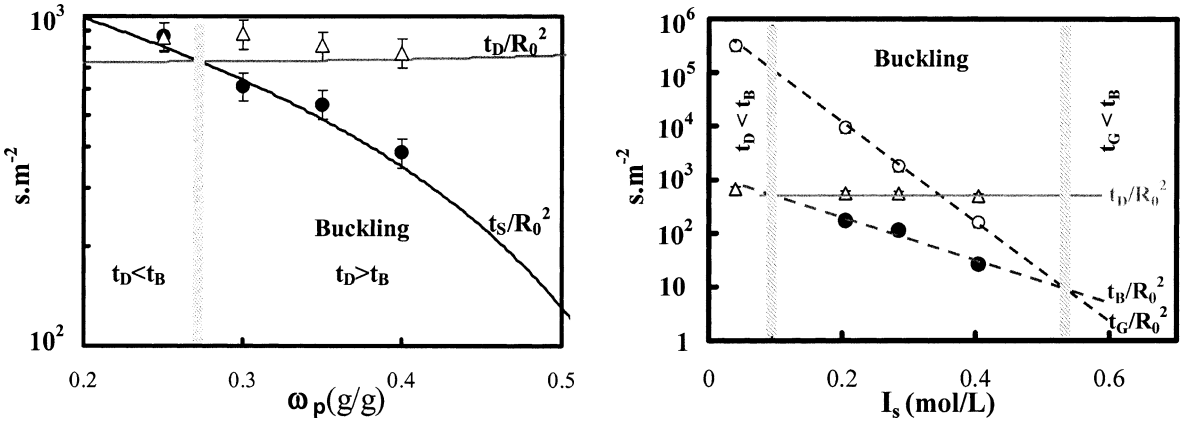

Fig. 5. Buckling instability characterizations: (a) Variations as a function of the polymer concentration, of t_D/R_0^2 (△: experimental measurements; grey line: model), of t_B/R_0^2 (•: experimental measurements) and of t_S/R_0^2 (dark line: theory) for sessile drops of dextran solutions; contact angle is $45 \pm 3°$. (b) Variations of t_B/R_0^2, t_D/R_0^2 and t_G/R_0^2 as a function of the ionic strength, I_s, for sessile drops of silica suspensions. The continue line comes from the model; the dashed lines only guide eyes; contact angles are $28 \pm 2°$.

simple evaluation of the local concentrations is not sufficient. In the following we simply compare the gelation time of the whole drop to the drying and buckling characteristic times. On one hand, if $t_G/t_D < 1$ the drop becomes gelled in its bulk before the end of drying (note that during a large part of the drying the interior of the drop keeps the same composition as the deposited suspension). For a buckling instability to occur, the interior of the drop has to be still liquid when the gelled skin forms at the drop surface. This will be satisfied only if t_G/t_D is not too small. Indeed if t_G/t_D is very small the interior of the drop gels before the accumulation of the particles and of the ionic species has had time to lead to a gelled skin (t_G is then smaller than t_B, see Fig. 5(b)). On the other hand, if $t_G/t_D > 1$ the drop is completely dried before the suspension has gelled. However, if t_G/t_D is not very large, the shortening of the gelation kinetics due to the accumulation of the particles and of the ionic species near the air/drop interface can be sufficient to lead to a gelled skin formation before the end of drying (t_D is then larger than t_B, see Fig. 5(b)); a buckling instability then takes place. On the contrary, if t_D is then smaller than t_B, as previously reported [2,12,17] particles and ionic species then accumulate near the three-phase line leading to the formation of a gelled 'foot' whereas the central part of the drop remains fluid. The comparison of the different characteristic times allows the analysis of our experimental results. The buckling instability only takes place when a gelled skin forms before the interior of the drop has completely dried or gelled, i.e., t_B smaller than t_D or t_G.

3.3. Secondary instability

Desiccation of a sessile drop when a gelled or glassy skin forms at its surface can also lead to secondary buckling instabilities displaying the different modes of deformation of an elastic shell. Observations have been done varying the geometrical parameters (contact base radius and contact angle) and the skin thickness which depends on the evaporation rate which is controlled by the relative humidity. Depending on the experimental conditions, various patterns are observed. In the case of a silica suspension drop, after the buckling instability described previously, we observe a collapse with an inversion of the curvature of the shell at its center. So, as shown on the top view reported in Fig. 6(a), a cascade of buckling which does not break the drop axisymmetry takes place. The picture in Fig. 6(a) corresponds to the final stage when the drop is completely gelled. Note that, in lateral views, the trough formed at the drop center is not visible; it appears as a zone of constant level in the profile (see Figs. 1 and 3).

In the case of dextran solutions, different behaviors are observed. We first consider the case of a drop with a usual contact angle (typically $\theta_0 = 30°$) but dried under a low relative humidity (RH = 30%). After the increase of the apex height, a breaking of the drop axisymmetry takes place leading to the formation of radial wrinkles as shown by the final top view in Fig. 6(b). The wrinkles number increases as the drop size, i.e., R_0, increases. We now consider the case of drops having a large contact angle (typically $\theta_0 = 70°$: such contact angles can be obtained using polyethylene substrates). The curvature at the apex is then larger than in the usual case (which corresponds to Fig. 3(b)). If the relative humidity is large (RH = 50%), the primary instability consists in an inversion of curvature at the center of the drop which leads to the formation of a circular fold (see Fig. 6(c)).

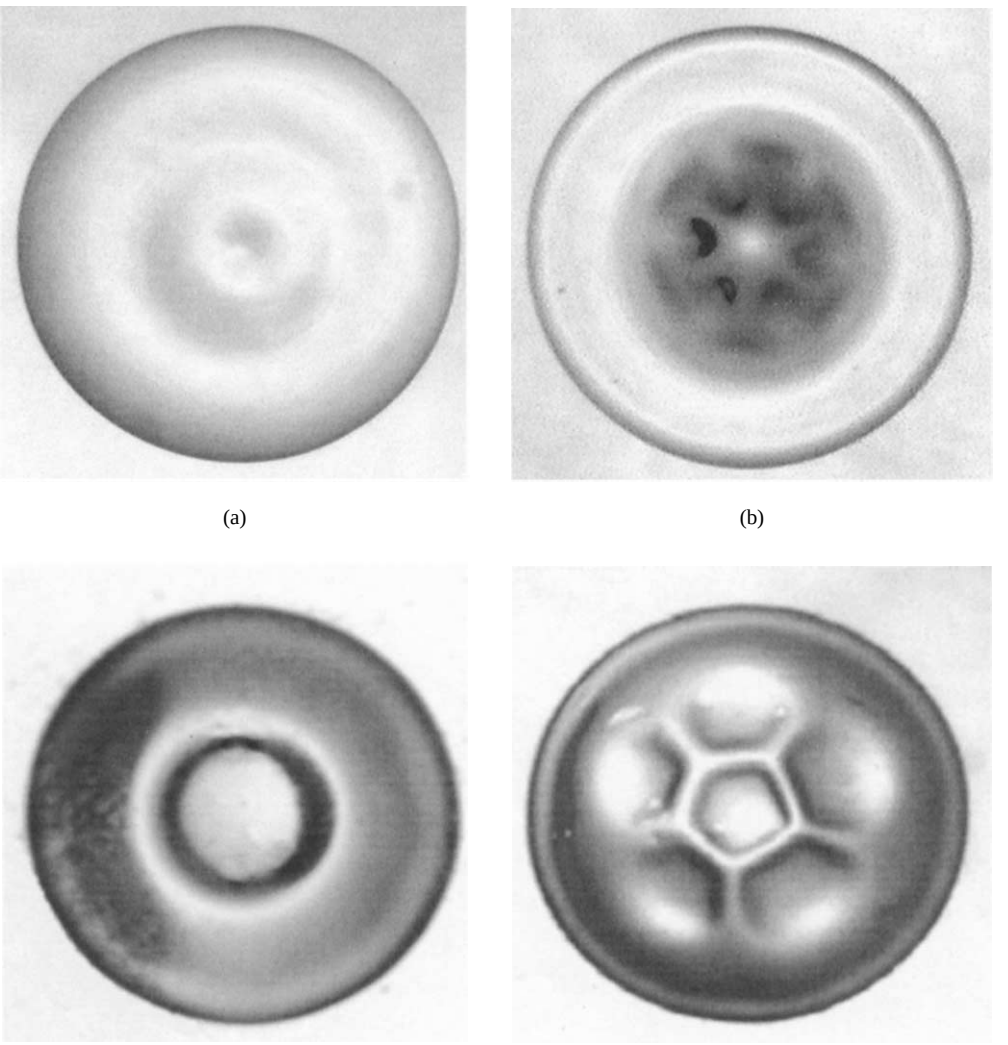

(a) (b)

(c) (d)

Fig. 6. Images of drops in top view: (a) Drop of silica suspension ($I_s = 0.21$ mol/L) after its collapse. (b) Drop of dextran solution ($\omega_p = 0.40$ g/g) dried at RH = 30%: radial wrinkles can be observed. (c) Drop of dextran solution ($\omega_p = 0.40$ g/g) having an initial contact angle equal to 70°: image was taken after the inversion of curvature of the drop central part leading to the formation of a trough. (d) Drop of dextran solution ($\omega_p = 0.40$ g/g) having an initial contact angle equal to 70° and dried at RH = 30%.

However, if the relative humidity is low (RH = 30%) as in Fig. 6(b), a more complex pattern progressively forms involving a cascade of buckling. The final state is shown in Fig. 6(d). Here also the drop axisymmetry is broken.

4. Conclusion

Desiccation of sessile drops of complex fluids can display large shape distortions. We studied such instabilities considering two different physico-chemical systems: colloidal particles suspensions and solutions of a polymer which becomes glassy for a sufficiently large polymer concentration. The shape evolution of the drops was found remarkably similar for the two systems. Experimental characterizations of the instability were done; in particular the time when the shape distortion begins has been measured as a function of the physicochemical conditions. The comparison of this time with the other characteristic times involved (drying time, gelation time, time of glassy skin formation) allows to show that the observed phenomenon is a buckling instability due to the formation of a permeable solid skin (gelled or glassy) at the drop surface which bends under

solvent evaporation. Moreover the comparison of the different times also allows to predict the conditions for a stable or instable shape evolution of the drop. Finally varying the experimental conditions secondary instabilities displaying different modes of deformation of an elastic shell have been observed.

References

[1] E. Adachi, A.S. Dimitrov, K. Nagayama, Langmuir 11 (1995) 1057.
[2] F. Parisse, C. Allain, J. Phys. II 6 (1996) 1111.
[3] R.D. Deegan, O. Bakajin, T.F. Dupont, G. Huber, S.R. Nagel, T.A. Witten, Nature 389 (1997) 827.
[4] R.D. Deegan, Phys. Rev. E 61 (2000) 475.
[5] R.D. Deegan, O. Bakajin, T.F. Dupont, G. Huber, S.R. Nagel, T.A. Witten, Phys. Rev. E 62 (2000) 756.
[6] K. Uno, K. Hayashi, T. Hayashi, K. Ito, H. Kitano, Colloid Polym. Sci. 276 (1998) 810.
[7] L. Shmuylovich, A.Q. Shen, H.A. Stone, Langmuir 18 (2002) 3441.
[8] J. Boneberg, F. Burmeister, C. Schäfle, P. Leiderer, Langmuir 13 (1997) 7080.
[9] T. Ondarçuhu, C. Joachim, Europhys. Lett. 42 (1998) 215.
[10] R. Blossey, A. Bosio, Langmuir 18 (2002) 2952.
[11] S.S. Abramchuk, A.R. Khokhlov, T. Iwataki, H. Oana, K. Yoshikawa, Europhys. Lett. 55 (2001) 234.
[12] F. Parisse, C. Allain, Langmuir 13 (1997) 3598.
[13] L. Pauchard, F. Parisse, C. Allain, Phys. Rev. E 59 (1999) 3737.
[14] H. Wang, Z. Wang, L. Huang, A. Mitra, Y. Yan, Langmuir 17 (2001) 2572.
[15] C.J. Martinez, J.A. Lewis, Langmuir 18 (2002) 4689.
[16] M.D. Haw, M. Gillie, W.C.K. Poon, Langmuir 18 (2002) 1626.
[17] F. Parisse, Thèse de l'Université Paris XI, Orsay, 1998.
[18] C.C. Annarelli, J. Fornazero, J. Bert, J. Colombani, Eur. Phys. J. E 5 (2001) 599.
[19] Z. Mitov, E. Kumachva, Phys. Rev. Lett. 81 (1998) 3427.
[20] P.G. de Gennes, Eur. Phys. J. E 6 (2001) 421.
[21] V.X. Nguyen, K.J. Stebe, Phys. Rev. Lett. 88 (2002) 164501.
[22] P. Parisse, C. Allain, Phys. Fluids 8 (1996) 9.
[23] P.G. de Gennes, Eur. Phys. J. E 7 (2001) 31.
[24] H. Vink, Eur. Polym. J. 7 (1971) 1411.
[25] D.J. Plazek, K.L. Ngai, The glass temperature, in: Physical Properties of Polymer Handbook, Part 12, AIP Press, 1996.
[26] L. Pauchard, C. Allain, Europhys. Lett., submitted.